

Power Control of Grid-Forming Converters Based on Full-State Feedback

Meng Chen, Dao Zhou, and Frede Blaabjerg

AAU Energy

Aalborg University

Aalborg, Denmark

mche@energy.aau.dk, zda@energy.aau.dk, fbl@et.aau.dk

Abstract—The active and reactive power controllers of grid-forming converters are traditionally designed separately, which relies on the assumption of loop decoupling. This paper proposes a full-state feedback control for the power loops of grid-forming converters. First, the power loops are modeled considering their natural coupling, which, therefore, can apply to all kinds of line impedance, i.e., resistive, inductive, or complex. Then a full-state feedback control design is used. By this way, the eigenvalues of the system can be arbitrarily placed to any positions in the timescale of power loops. Therefore, the parameters can be directly chosen by the predefined specifications. A step-by-step parameters design procedure is also given in this paper. Experimental results verify the proposed method.

Index Terms—full-state feedback control, grid-forming converter, loop coupling, controllability, line impedance

I. INTRODUCTION

The control-based grid-forming converters are becoming vital to the power system due to their ability to help stabilize the frequency and voltage. The control system of the grid-forming converters is typically complicated with multiple loops, e.g., cascaded voltage and current loops, active and reactive power loops. To simplify the analysis and design, the cascaded loops are usually designed with higher bandwidths than those of the power loops. As a result, the quick dynamics of the cascaded loops can be neglected when focusing on the power loops [1]. Moreover, the frequency and voltage are also assumed to be independently controlled by the active and reactive powers, respectively [2]. Popular control strategies of such grid-forming converters are the droop control and the virtual synchronous generator control [3]–[5].

However, the coupling between the active and reactive power loops is highly related to the line impedance. In a resistive grid, the frequency is more influenced by the reactive power, and the voltage is more related to the active power, which is opposite with the condition of a inductive grid [6]. Furthermore, for a complex impedance, the frequency, voltage, active and reactive powers have strong relations, where the active and reactive power loops are not supposed to be decoupled. The virtual impedance is a typical method to strengthen the decoupling between the active and reactive

powers, which should be designed carefully to obtain a favorable performance [7]. Nevertheless, even in a inductive grid, the decoupling between the active and reactive power loops may need additional restraints [8]. Meanwhile, the decoupling is just an approximate rather than exact result. In conclusion, the decoupling-based power control may not provide a robust structure for the grid-forming converters. To get rid of the assumption of power decoupling, the multivariable feedback-based grid-forming converters have been proposed, which can simultaneously tunes both the active and reactive power loops [9], [10].

The parameters design of the power control is of great importance to the grid-forming converters in order to well behave the advantages and provide a superior performance. The traditional method is based on the classic control, e.g., root locus analysis, frequency analysis, etc [11], [12]. These methods may be complicated when dealing with multiple loops and parameters like coupled active and reactive power loops in the grid-forming converters as they can only study the single-input single-output system with one adjustable parameters at a time.

In this paper, a full-state feedback based-power control is proposed for the grid-forming converters. With this method, the following advantages can be achieved.

- 1) The model considers the natural coupling between the active and reactive power loops without decoupling assumptions. Therefore, the control structure is effective to any kinds of line impedance, i.e., resistive, inductive, or complex.
- 2) The close-loop eigenvalues of the power loops can be arbitrarily placed to any positions in the timescale of power loops.
- 3) A step-by-step parameters design procedure based on the proposed method is provided.

The remainder of paper is organized as follows. The model of the grid-forming converter power loops is built in Section II. In Section III, the details of the full-state feedback-based power control is given. In Section IV, experimental results are shown, and finally, conclusions are given in Section V.

This work was supported by the Reliable Power Electronic-Based Power System (REPEPS) project at the Department of Energy Technology, Aalborg University as part of the Villum Investigator Program funded by the Villum Foundation.

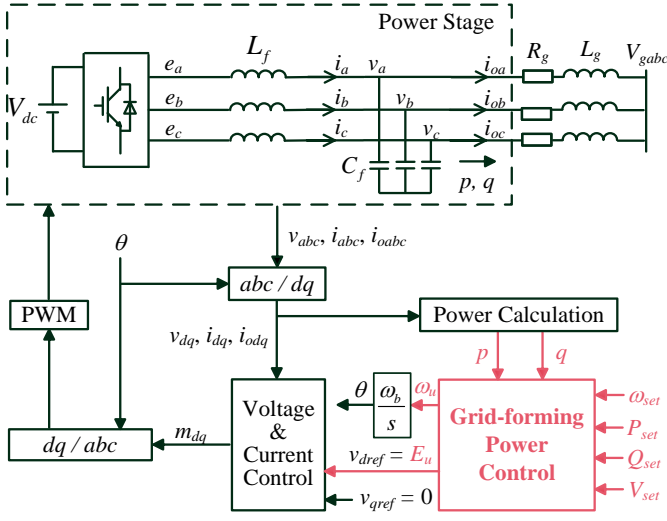


Fig. 1. General configuration of grid-forming converters.

II. MODELING OF GRID-FORMING CONVERTERS POWER LOOPS

Fig. 1 shows the general configuration of a power converter controlled by the grid-forming power controller with the cascaded voltage and current loops. A three-phase converter is connected to the power grid via an LC filter, where L_f and C_f are the filter inductor and capacitor, respectively. L_g and R_g are the inductor and resistor of the line to the power grid, where both of them will be included into the modeling to represent all kinds of line impedance. The grid-forming power control copes with the output active and reactive powers of the converter, p and q , to provide the frequency and voltage references, i.e., ω_u and E_u .

When considering a general line impedance, the output active and reactive powers of the power converter can be expressed as [13]

$$p = \frac{V^2 R_g + V V_g (X_g \sin \delta - R_g \cos \delta)}{R_g^2 + X_g^2} \quad (1)$$

$$q = \frac{V^2 X_g - V V_g (R_g \sin \delta + X_g \cos \delta)}{R_g^2 + X_g^2} \quad (2)$$

where V and V_g are the voltage magnitudes of the capacitor and grid, respectively. Moreover, δ is the power angle, which is defined as

$$\delta = \omega_b \omega - \omega_b \omega_g \quad (3)$$

where ω and ω_g are the voltage frequencies of the capacitor and grid, and ω_b is the base value of the frequency.

According to (1)-(3), the small-signal model of the output powers can be derived as

$$\Delta p = K_{p\delta} \Delta \delta + K_{pV} \Delta V \quad (4)$$

$$\Delta q = K_{q\delta} \Delta \delta + K_{qV} \Delta V \quad (5)$$

$$\Delta \dot{\delta} = \omega_b \Delta \omega \quad (6)$$

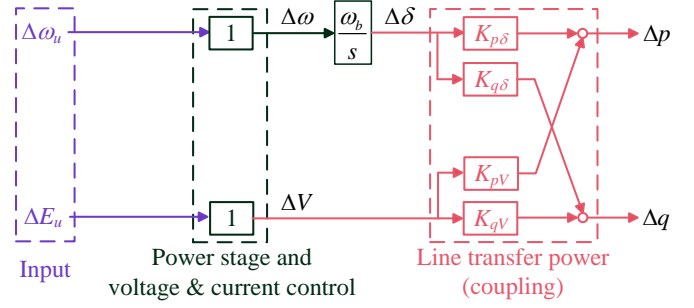


Fig. 2. Open-loop small-signal model of power loops.

where

$$K_{p\delta} = \left. \frac{\partial p}{\partial \delta} \right|_{\delta_0, V_0} = \frac{V_0 V_g (R_g \sin \delta_0 + X_g \cos \delta_0)}{R_g^2 + X_g^2} \quad (7)$$

$$K_{pV} = \left. \frac{\partial p}{\partial V} \right|_{\delta_0, V_0} = \frac{2V_0 R_g + V_g (X_g \sin \delta_0 - R_g \cos \delta_0)}{R_g^2 + X_g^2} \quad (8)$$

$$K_{q\delta} = \left. \frac{\partial q}{\partial \delta} \right|_{\delta_0, V_0} = \frac{V_0 V_g (X_g \sin \delta_0 - R_g \cos \delta_0)}{R_g^2 + X_g^2} \quad (9)$$

$$K_{qV} = \left. \frac{\partial q}{\partial V} \right|_{\delta_0, V_0} = \frac{2V_0 X_g - V_g (R_g \sin \delta_0 + X_g \cos \delta_0)}{R_g^2 + X_g^2} \quad (10)$$

and the subscript "0" represent the variables corresponding to the used steady-state operation point to linearize the model. Apparently, both the active and reactive powers are related not only to $\Delta \delta$ but also to ΔV if considering a general line impedance.

Due to the much larger bandwidths of the cascaded loops, their quick dynamics can be neglected, which yields

$$\begin{bmatrix} \Delta \omega \\ \Delta V \end{bmatrix} = \begin{bmatrix} \Delta \omega_u \\ \Delta E_u \end{bmatrix} \quad (11)$$

Combining (4)-(6) and (11), the open-loop small-signal model of the grid-forming converter power loops can be graphically shown in Fig. 2. As observed, the active and reactive power loops are coupled with each other for a general line impedance.

Usually, a droop control is preferred to be included in the grid-forming control due to the potential islanded operation after various disturbances. A typical choice of the droop characteristics can be expressed as

$$\omega_u - \omega_{set} = D_p (P_{set} - p) \quad (12)$$

$$V - V_{set} = D_q (Q_{set} - q) \quad (13)$$

where D_p and D_q are the droop coefficients, the subscript "set" represents the variables corresponding to the set-point. Motivated from this, two new small-signal outputs are defined as

$$\begin{bmatrix} y_1 \\ y_2 \end{bmatrix} = \begin{bmatrix} \Delta \omega_u + D_p \Delta p \\ \Delta V + D_q \Delta q \end{bmatrix} \quad (14)$$

where their references are defined as

$$\begin{bmatrix} y_{1ref} \\ y_{2ref} \end{bmatrix} = \begin{bmatrix} \Delta \omega_{set} + D_p \Delta P_{set} \\ \Delta V_{set} + D_q \Delta Q_{set} \end{bmatrix} \quad (15)$$

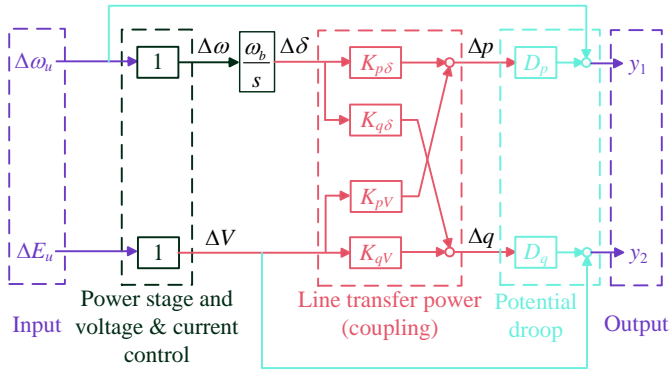


Fig. 3. Extended open-loop small-signal model of power loops with droop characteristics.

By including (14), the open-loop small-signal model in Fig. 2 is extended to Fig. 3. As shown, it is a coupled two-input two-output system, where the state-space representation can be derived as

$$\Delta \dot{\delta} = [\omega_b \quad 0] \begin{bmatrix} \Delta \omega_u \\ \Delta E_u \end{bmatrix} \quad (16)$$

$$\begin{bmatrix} y_1 \\ y_2 \end{bmatrix} = \begin{bmatrix} D_p k_{p\delta} \\ D_q k_{q\delta} \end{bmatrix} \Delta \delta + \begin{bmatrix} 1 & D_p k_{pV} \\ 0 & 1 + D_q k_{qV} \end{bmatrix} \begin{bmatrix} \Delta \omega_u \\ \Delta E_u \end{bmatrix} \quad (17)$$

Therefore, the control target for the is to design proper close-loop controllers so that the the outputs $[y_1 \ y_2]^T$ of the open-loop system represented by (16) and (17) can track the references $[y_{ref1} \ y_{ref2}]^T$ with zero steady-state errors by favorable dynamics. In the following, it will show that the full-state feedback can well solve the problem.

III. FULL-STATE FEEDBACK CONTROL DESIGN

A. Control Law Construction

To evaluate the errors between the references and the outputs, the following variables are defined.

$$\begin{bmatrix} e_1 \\ e_2 \end{bmatrix} = \begin{bmatrix} y_1 - y_{1ref} \\ y_2 - y_{2ref} \end{bmatrix} \quad (18)$$

As the references of (15) are usually step disturbances, the derivatives of the errors can be derived as

$$\begin{bmatrix} \dot{e}_1 \\ \dot{e}_2 \end{bmatrix} = \begin{bmatrix} \dot{y}_1 \\ \dot{y}_2 \end{bmatrix} \quad (19)$$

Placing (17) into (19) yields

$$\begin{bmatrix} \dot{e}_1 \\ \dot{e}_2 \end{bmatrix} = \begin{bmatrix} D_p k_{p\delta} \\ D_q k_{q\delta} \end{bmatrix} \Delta \dot{\delta} + \begin{bmatrix} 1 & D_p k_{pV} \\ 0 & 1 + D_q k_{qV} \end{bmatrix} \begin{bmatrix} \Delta \dot{\omega}_u \\ \Delta \dot{E}_u \end{bmatrix} \quad (20)$$

Define the following intermediate variables

$$z = \Delta \delta, \quad \begin{bmatrix} u_1 \\ u_2 \end{bmatrix} = \begin{bmatrix} \Delta \dot{\omega}_u \\ \Delta \dot{E}_u \end{bmatrix} \quad (21)$$

where (20) can, therefore, be rewritten as

$$\begin{bmatrix} \dot{e}_1 \\ \dot{e}_2 \end{bmatrix} = \begin{bmatrix} D_p k_{p\delta} \\ D_q k_{q\delta} \end{bmatrix} z + \begin{bmatrix} 1 & D_p k_{pV} \\ 0 & 1 + D_q k_{qV} \end{bmatrix} \begin{bmatrix} u_1 \\ u_2 \end{bmatrix} \quad (22)$$

Moreover, according to the definition of z in (21), its derivative is

$$\dot{z} = \Delta \ddot{\delta} \quad (23)$$

which can, combining with (16), be rewritten as

$$\dot{z} = [\omega_b \quad 0] \begin{bmatrix} \Delta \dot{\omega}_u \\ \Delta \dot{E}_u \end{bmatrix} \quad (24)$$

Afterwards, the dynamics of z can be determined by placing (21) into (24) as

$$\dot{z} = [\omega_b \quad 0] \begin{bmatrix} u_1 \\ u_2 \end{bmatrix} \quad (25)$$

Therefore, the extended state differential equations of the power loops can, by taking (22) and (25) together, be derived as

$$\begin{bmatrix} \dot{e}_1 \\ \dot{e}_2 \\ \dot{z} \end{bmatrix} = \mathbf{A} \begin{bmatrix} e_1 \\ e_2 \\ z \end{bmatrix} + \mathbf{B} \begin{bmatrix} u_1 \\ u_2 \end{bmatrix} \quad (26)$$

where

$$\mathbf{A} = \begin{bmatrix} 0 & 0 & D_p k_{p\delta} \\ 0 & 0 & D_q k_{q\delta} \\ 0 & 0 & 0 \end{bmatrix}, \quad \mathbf{B} = \begin{bmatrix} 1 & D_p k_{pV} \\ 0 & 1 + D_q k_{qV} \\ \omega_b & 0 \end{bmatrix} \quad (27)$$

According to the full-state feedback theory [14], the eigenvalues of the close-loop system can be placed to anywhere by the following control law if the open-loop system (\mathbf{A}, \mathbf{B}) is completely controllable.

$$\begin{bmatrix} u_1 \\ u_2 \end{bmatrix} = -\mathbf{K} \begin{bmatrix} e_1 \\ e_2 \\ z \end{bmatrix} \quad (28)$$

where

$$\mathbf{K} = \begin{bmatrix} k_{11} & k_{12} & k_{13} \\ k_{21} & k_{22} & k_{23} \end{bmatrix} \quad (29)$$

and the open-loop system (\mathbf{A}, \mathbf{B}) is completely controllable if the following defined controllability matrix \mathbf{P} has

$$\text{rank}(\mathbf{P}) = 3 \quad (30)$$

and

$$\mathbf{P} \triangleq [\mathbf{B} \quad \mathbf{A}\mathbf{B} \quad \mathbf{A}^2\mathbf{B}] = \begin{bmatrix} 1 & D_p k_{pV} & \omega_b D_p k_{p\delta} & 0 & 0 & 0 \\ 0 & 1 + D_q k_{qV} & \omega_b D_q k_{q\delta} & 0 & 0 & 0 \\ \omega_b & 0 & 0 & 0 & 0 & 0 \end{bmatrix} \quad (31)$$

Finally, by placing (28) back into (21), the actual inputs provided by the grid-forming power control can be derived as

$$\begin{bmatrix} \Delta \omega_u \\ \Delta E_u \end{bmatrix} = \int_0^t \left(\begin{bmatrix} k_{11} & k_{12} \\ k_{21} & k_{22} \end{bmatrix} \begin{bmatrix} -e_1 \\ -e_2 \end{bmatrix} \right) d\tau - \begin{bmatrix} k_{13} \\ k_{23} \end{bmatrix} \Delta \delta \quad (32)$$

Therefore, the complete close-loop small-signal model of the proposed grid-forming converter can be shown in Fig. 4.

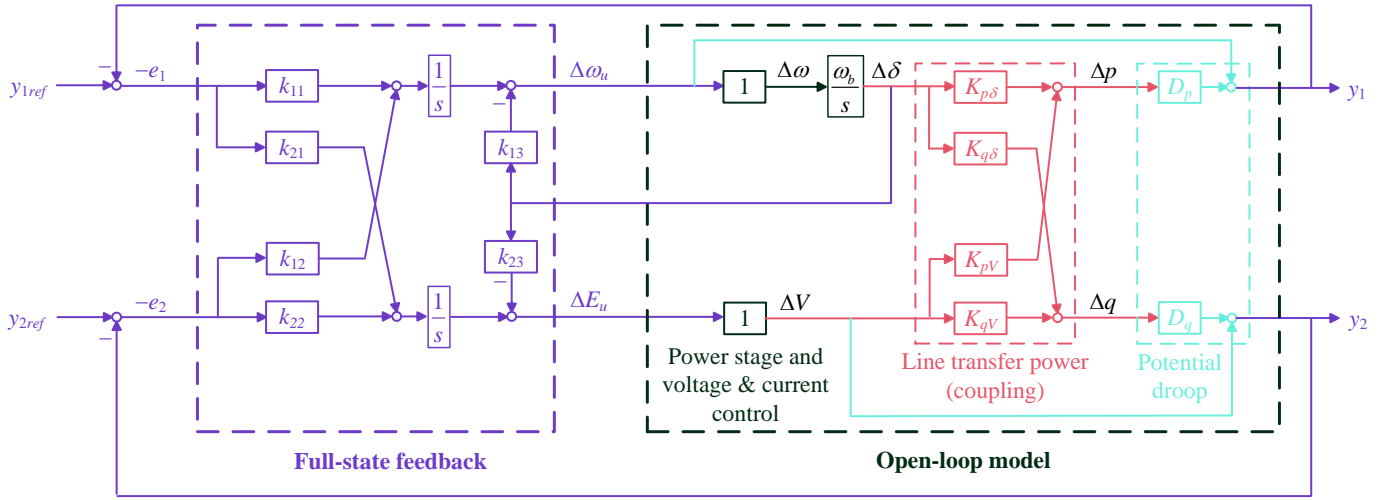


Fig. 4. Close-loop small-signal model of proposed grid-forming converter.

B. Parameters Design

By applying the full-state feedback control law of (28), the close-loop dynamics of (26) is derived as

$$\begin{bmatrix} \dot{e}_1 \\ \dot{e}_2 \\ \dot{z} \end{bmatrix} = (\mathbf{A} - \mathbf{BK}) \begin{bmatrix} e_1 \\ e_2 \\ z \end{bmatrix} \quad (33)$$

where its characteristic equation is

$$|\lambda \mathbf{I} - \mathbf{A} + \mathbf{BK}| = 0 \quad (34)$$

The characteristic equation (34) has three eigenvalues, which can be placed in anywhere. As a reasonable choice, we choose a pair of complex eigenvalue as the dominant ones and a real eigenvalue, which is far away from the dominant eigenvalues. Therefore, the characteristic equation should has the following form

$$(\lambda + a)(\lambda^2 + 2\xi\omega_n\lambda + \omega_n^2) = 0 \quad (35)$$

where $-a$ is the chosen real eigenvalue, ξ and ω_n are the damping ratio and natural frequency of the chosen complex eigenvalues. Thereafter, the parameters (29) can be solved by

$$|\lambda \mathbf{I} - \mathbf{A} + \mathbf{BK}| \equiv (\lambda + a)(\lambda^2 + 2\xi\omega_n\lambda + \omega_n^2) \quad (36)$$

It should be mentioned that (30) guarantees that (36) must have solutions. Meanwhile, ξ and ω_n are directly related to the time domain performance, e.g., overshoot, settle time, etc., which can, therefore, be used to determine the dominant complex eigenvalues.

According to the aforementioned discussion, a step-by-step parameter design procedure can be given as follows.

- step 1: Choose the steady-state operation point to linearize the system.
- step 2: Calculate $K_{p\delta}$, K_{pV} , $K_{q\delta}$, and K_{qV} of the chosen steady-state operation point based on (7)-(10).
- step 3: Calculate the matrices \mathbf{A} and \mathbf{B} of (27).

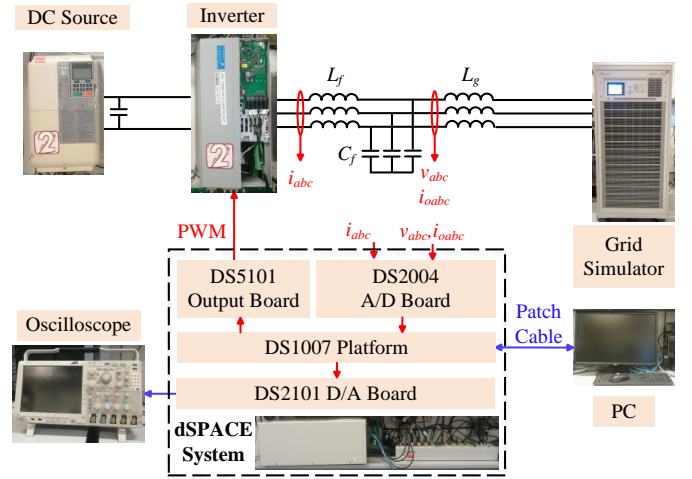


Fig. 5. Experimental configuration of grid-forming converter.

- step 4: Check the controllability according to (30) and (31).
- step 5: Choose proper eigenvalues according to the requirements of the time domain performance.
- step 6: Solve (36) to obtain the parameter matrix \mathbf{K} .

IV. EXPERIMENTAL VALIDATION

To verify the proposed full-state feedback control for power loops of the grid-forming converter as well as the step-by-step parameter design procedure, this section will present corresponding experimental results. The configuration of the setup is shown in Fig. 5, and the key parameters are given in Table I.

The step-by-step parameter design procedure is applied as follows.

- step 1: Choose the steady-state operation point to linearize the system.

The steady-state operation point with the parameters in Table I is $(\delta_0, V_0) = (0.0435, 0.9997)$.

TABLE I
PARAMETERS OF EXPERIMENTAL SETUPS

Symbol	Description	Value
f_n	Nominal frequency	100π rad/s
S_n	Nominal power	5 kW
V_n	Nominal line-to-line RMS voltage	380 V
f_{sw}	Switching frequency	10 kHz
ω_g	Grid frequency	100π rad/s (1 p.u.)
V_g	Line-to-line RMS grid voltage	380 V (1 p.u.)
L_g	Line inductor	8 mH (0.087 p.u.)
C_f	Filter capacitor	$5 \mu\text{F}$ (0.0454 p.u.)
L_f	Filter inductor	3 mH (0.0326 p.u.)
D_p	Droop coefficient of P - f regulation	0.01 p.u.
D_q	Droop coefficient of Q - V regulation	0.05 p.u.
ω_{set}	Frequency reference	1 p.u.
P_{set}	Active power reference	0.5 p.u.
Q_{set}	Reactive power reference	0 p.u.
V_{set}	Voltage magnitude reference	1 p.u.

- step 2: Calculate $K_{p\delta}$, K_{pV} , $K_{q\delta}$, and K_{qV} of the chosen steady-state operation point based on (7)-(10).

The corresponding parameters are calculated as $(K_{p\delta}, K_{pV}, K_{q\delta}, K_{qV}) = (11.4761, 0.5002, 0.5, 11.4939)$.

- step 3: Calculate the matrices \mathbf{A} and \mathbf{B} of (27).

The corresponding matrices are calculated as

$$\mathbf{A} = \begin{bmatrix} 0 & 0 & 0.1148 \\ 0 & 0 & 0.025 \\ 0 & 0 & 0 \end{bmatrix}, \mathbf{B} = \begin{bmatrix} 1 & 0.005 \\ 0 & 1.5747 \\ 314.1593 & 0 \end{bmatrix} \quad (37)$$

- step 4: Check the controllability according to (30) and (31).

The controllability matrix is calculated as

$$\mathbf{P} = \begin{bmatrix} 1 & 0.005 & 36.0533 & 0 & 0 & 0 \\ 0 & 1.5747 & 7.854 & 0 & 0 & 0 \\ 314.1593 & 0 & 0 & 0 & 0 & 0 \end{bmatrix} \quad (38)$$

where it is easy to check that $\text{rank}(\mathbf{P}) = 3$. Therefore, the system (\mathbf{A}, \mathbf{B}) is completely controllable.

- step 5: Choose proper eigenvalues according to the requirements of the time domain performance.

As an example, in this paper, we consider the percent overshoot ($P.O.$) and settle time (T_s) as the performance indices, where they are related to ξ and ω_n by the following equations [15].

$$P.O. = e^{-(\xi/\sqrt{1-\xi^2})} \times 100\% \quad (39)$$

$$T_s = \frac{4}{\xi\omega_n} \quad (40)$$

For comparison, this paper choose four cases as shown in Table II, where the third eigenvalue a is always placed far away from the dominant complex eigenvalues. The corresponding positions of the dominant eigenvalues are shown in Fig. 6.

TABLE II
STUDIED CASES TO PLACE EIGENVALUES

Cases	Damping Ratio ξ	Settle Time T_s	Third eigenvalue a
1	0.4	1 s	-20
2	0.4	2 s	-20
3	0.707	1 s	-20
4	0.707	2 s	-20

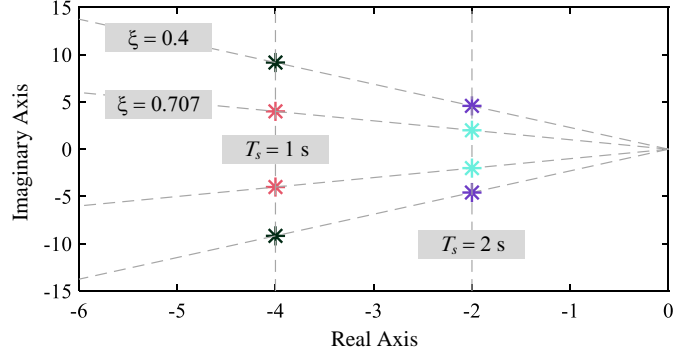


Fig. 6. Chosen dominant complex eigenvalues.

TABLE III
DESIGNED PARAMETERS OF THE CORRESPONDING CASES

Parameters	Case 1	Case 2	Case 3	Case 4
k_{11}	2.7756	0.6939	0.8885	0.2221
k_{12}	-0.0088	-0.0022	-0.0028	-0.0007
k_{13}	0.0166	0.0105	0.0226	0.012
k_{21}	0.0367	0.0389	0.0385	0.0399
k_{22}	12.7007	12.7007	12.7007	12.7007
k_{23}	0.0161	0.0161	0.0161	0.0161

- step 6: Solve (36) to obtain the parameter matrix \mathbf{K} .

The designed parameters corresponding to the four cases are listed in Table III.

Fig. 7 presents the experimental comparisons of the studied cases when P_{set} steps from 0.5 p.u. to 1 p.u.. As shown, when choosing a large damping ratio ($\xi = 0.707$ in Case 3 and Case 4), the dynamics have smaller $P.O.$ than those with a small damping ratio ($\xi = 0.4$ in Case 1 and Case 2). Meanwhile, when choosing a small settle time ($T_s = 1$ s in Case 1 and Case 3), the systems can reach to the steady-state quicker than those with a large settle time ($T_s = 2$ s in Case 2 and Case 4). Fig. 7 proves that the proposed full-state back control structure and parameter design method are effective to regulate the power loops of the grid-forming converter to satisfy the predefined time domain performance.

V. CONCLUSION

This paper proposes a new control structure of the grid-forming converter power loops based on the full-state feedback

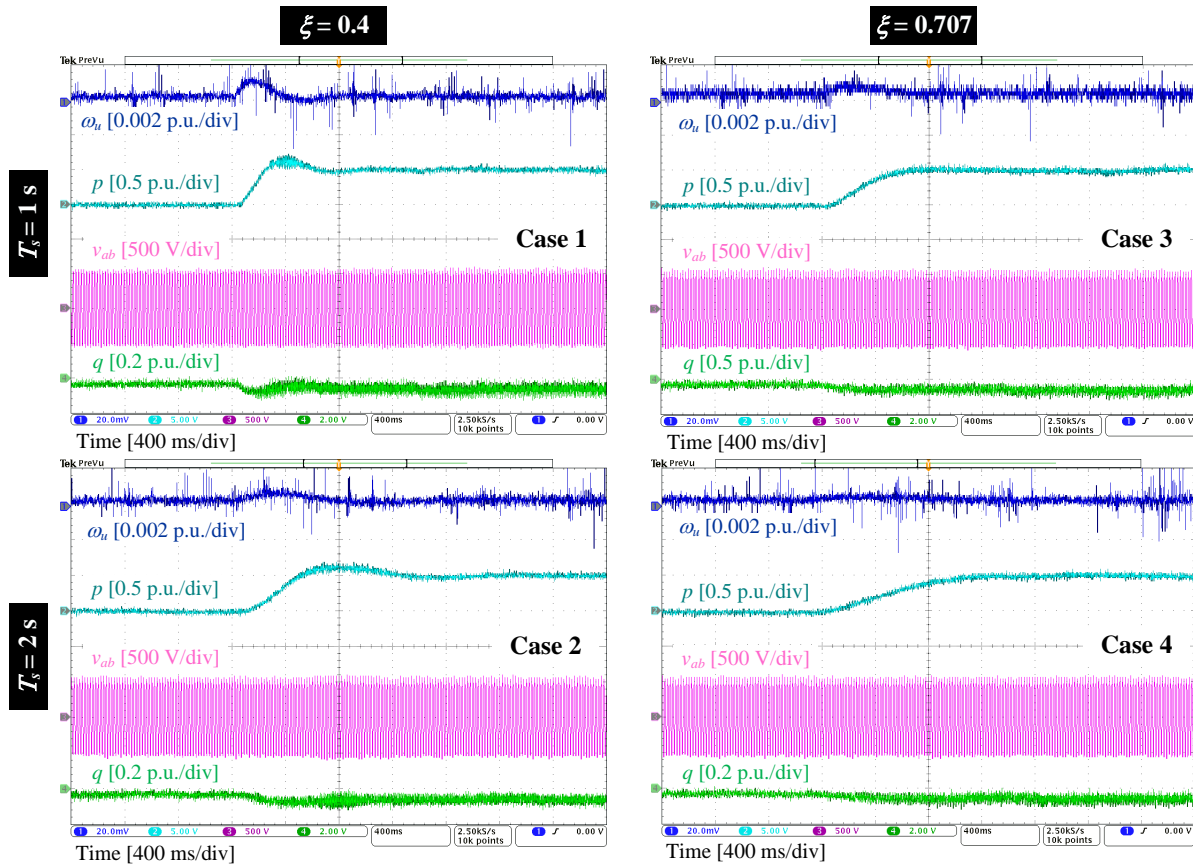


Fig. 7. Experimental results of studies cased when P_{ref} steps from 0.5 p.u. to 1 p.u.

control. The modeling considers a general line impedance and the coupling between the power loops, which makes that the proposed control can be applied to a inductive, resistive, or complex grid line. A step-by-step parameter design procedure is given as well, where the eigenvalues can be placed anywhere within the timescale of the power loops. By this way, the control parameters can be directly calculated based on the predefined time domain indices, which are verified by the experimental results.

REFERENCES

- [1] R. Rosso, X. Wang, M. Liserre, X. Lu, and S. Engelken, "Grid-forming converters: Control approaches, grid-synchronization, and future trends—a review," *IEEE Open J. Ind. Appl.*, vol. 2, pp. 93–109, Apr. 2021.
- [2] A. Tayyebi, D. Gross, A. Anta, F. Kupzog, and F. Dörfler, "Frequency stability of synchronous machines and grid-forming power converters," *IEEE J. Emerg. Sel. Top. Power Electron.*, vol. 8, no. 2, pp. 1004–1018, Jun. 2020.
- [3] M. Chen, D. Zhou, C. Wu, and F. Blaabjerg, "Characteristics of parallel inverters applying virtual synchronous generator control," *IEEE Trans. Smart Grid*, vol. 12, no. 6, pp. 4690–4701, Nov. 2021.
- [4] H. Zhang, W. Xiang, W. Lin, and J. Wen, "Grid forming converters in renewable energy sources dominated power grid: Control strategy, stability, application, and challenges," *J. Mod. Power Syst. Clean Energy*, vol. 9, no. 6, pp. 1239–1256, Nov. 2021.
- [5] M. Chen, D. Zhou, and F. Blaabjerg, "Enhanced transient angle stability control of grid-forming converter based on virtual synchronous generator," *IEEE Trans. Ind. Electron.*, vol. 69, no. 9, pp. 9133–9144, Sep. 2022.
- [6] F. Deng, Y. Li, X. Li, W. Yao, X. Zhang, and P. Mattavelli, "A decentralized impedance reshaping strategy for balanced, unbalanced and harmonic power sharing in islanded resistive microgrids," *IEEE Trans. Sustain. Energy*, vol. 13, no. 2, pp. 743–754, Apr. 2022.
- [7] M. Ahmed, L. Meegahapola, A. Vahidnia, and M. Datta, "Adaptive virtual impedance controller for parallel and radial microgrids with varying X/R ratios," *IEEE Trans. Sustain. Energy*, vol. 13, no. 2, pp. 830–843, Apr. 2022.
- [8] H. Wu, X. Ruan, D. Yang, X. Chen, W. Zhao, Z. Lv, and Q.-C. Zhong, "Small-signal modeling and parameters design for virtual synchronous generators," *IEEE Trans. Ind. Electron.*, vol. 63, no. 7, pp. 4292–4303, Jul. 2016.
- [9] L. Huang, H. Xin, and F. Dörfler, " \mathcal{H}_∞ -control of grid-connected converters: Design, objectives and decentralized stability certificates," *IEEE Trans. Smart Grid*, vol. 11, no. 5, pp. 3805–3816, Sep. 2020.
- [10] M. Chen, D. Zhou, A. Tayyebi, E. Prieto-Araujo, F. Dörfler, and F. Blaabjerg, "Generalized multivariable grid-forming control design for power converters," *IEEE Trans. Smart Grid*, pp. 1–1, 2022.
- [11] J. Chen and T. O'Donnell, "Parameter constraints for virtual synchronous generator considering stability," *IEEE Trans. Power Syst.*, vol. 34, no. 3, pp. 2479–2481, May 2019.
- [12] M. Chen, D. Zhou, and F. Blaabjerg, "Active power oscillation damping based on acceleration control in paralleled virtual synchronous generators system," *IEEE Trans. Power Electron.*, vol. 36, no. 8, pp. 9501–9510, Aug. 2021.
- [13] N. Mohammed and M. Ciobotaru, "Adaptive power control strategy for smart droop-based grid-connected inverters," *IEEE Trans. Smart Grid*, pp. 1–1, 2022.
- [14] R. C. Dorf and R. H. Bishop, *Modern Control Systems*. Prentice Hall, 2010.
- [15] K. Ogata, *Modern Control Engineering*. Prentice Hall, 2009.